JOURNAL OF AIRCRAFT
Vol. 48, No. 2, March–April 2011

Engineering Notes

Euler Calculation of Rotor–Airframe Interaction Based on Unstructured Overset Grids

He-yong Xu* and Zheng-yin Ye†
Northwestern Polytechnical University, Xi'an 710072, People's Republic of China

DOI: 10.2514/1.C031051

Nomenclature

$C_{p,\text{inst}}$	=	instantaneous coefficient of pressure
$C_{p,\text{mean}}$	=	time-averaged pressure coefficient
C_T	=	thrust coefficient of the rotor
U	=	streamwise velocity component, m/s
V_{ABCD}	=	volume of tetrahedron $ABCD$
V_0	=	velocity of the coming freestream, m/s
W	=	downward velocity component, m/s
W_A, W_B, W_C, W_D	=	flow variables of mesh points A, B, C, and D
w	=	downwash velocity, m/s
Ψ	=	azimuth angle of the rotor

I. Introduction

IN CURRENT computational fluid dynamics (CFD), prediction of the helicopter rotor–airframe unsteady aerodynamic interaction is regarded as one of the most challenging problems. In the past two decades, several studies were conducted for the simulation of this complicated flow problem. In [1,2], singularity methods such as lifting-line/free-wake methods were used to model the rotor blade and the airframe. In [3,4], Euler and Navier–Stokes equations were used to simulate the time-averaged flowfield, and the rotors were modeled as a momentum source. An alternative way of predicting time-averaged rotor–airframe interaction aerodynamics was also proposed by modeling the rotor as an actuator disk [5]. This actuator disk model was also adopted in unstructured mesh flow solvers for rotor–airframe interaction studies [6,7]. An extension of the actuator disk model was made for the prediction of unsteady inflow and airframe surface pressure by combining the generalized dynamic wake theory with an overset-grid Navier–Stokes flow solver [8]. A disk model with distributed source coupled with a parallel Navier–Stokes flow solver was also used for the simulation of unsteady rotor–airframe interaction aerodynamics [9]. However, the methods based on momentum source or actuator disk model are unable to predict details of the induced velocity field. Recently, structured overset-grid methods have been used to handle the relative motion between the rotor blades and the airframe [10].

Received 6 April 2010; revision received 12 November 2010; accepted for publication 12 November 2010

*Postdoctoral Researcher, National Key Laboratory of Science and Technology on Aerodynamic Design and Research; xhy2005@mail.nwpu.edu.cn.

†Professor, National Key Laboratory of Science and Technology on Aerodynamic Design and Research; yezy@nwpu.edu.cn.

CFD methods based on unstructured meshes have an advantage of easily handling complex geometries, and the unstructured mesh technique was successfully applied to solve the flow around rotor-alone configurations [11]. Recently, the unstructured mesh method was extended for the efficient simulation of helicopter rotor–airframe flowfield [12], and adaptive meshing, rotor trim, low Mach precondition, and sliding mesh were used to solve the unsteady Euler equations. In the present study, a technique of unstructured overset grids is developed for the time-accurate simulation of rotor–airframe interaction aerodynamics. The relative motion between the rotor blades and the airframe is treated by dividing the flow domain into two zones: the rotational subzone and the stationary subzone. The rotational subzone contains the rotors and rotates with it, and the stationary subzone contains the airframe. This method is validated by calculating the time-averaged and unsteady flowfields around the Georgia Institute of Technology (Georgia Tech) rotor–airframe configuration and comparing the results with experimental data and calculating results from [12].

II. Unstructured Overset-Grid Method

A. Construction of Unstructured Overset Grids

The Georgia Tech rotor–airframe configuration is shown in Fig. 1a. To generate appropriate overset girds, we first need to set two restriction boundary surfaces (as shown in Fig. 1b: surfaces 2 and 3. The two surfaces are cylindrical, which are centered on the rotation axis. Then we generated three part domain meshes: namely, mesh between rotor blades surface 1 and restriction boundary surface 2, mesh between the two restriction boundary surfaces 2 and 3, and mesh among restriction boundary surface 3 and airframe surface 4 and the far-field boundary. Finally, we obtained a whole unstructured mesh.

The overset grids consist of two subzones: rotational subzone and stationary subzone. The rotational subzone is the computational domain between the rotor blades surface 1 and the restriction boundary surface 3, which contains the rotor blades and rotates with them. The stationary subzone is the computational domain among the airframe surface 4 and the restriction boundary surface 2 and the far-field boundary, which contains the airframe. The domain between restriction boundary surfaces 2 and 3 is the overlapping zone, which is used to couple the flow variables of two subzones.

B. Searching for the Donor Elements

During the unsteady simulation, the locations of the rotational grid elements vary with time relative to the stationary mesh, and we must update the donor elements for all artificial boundary points at every time stage.

For the purpose of convenient viewing, a 2-D map of coarse overset grids is given in Fig. 2a. The $\Delta A'B'C'$ is a triangle on the artificial boundary of the rotational subdomain, and its center point P' is the point whose flow variables are needed to be interpolated from its donor element. The over-striking triangles are all the artificial boundary triangles. From the above method of overset-grid formation, we know that the $\Delta A'B'C'$ superposes with the triangle ΔABC in the stationary subdomain mesh, and the point P' also superposes with the center point P of the ΔABC. So the initial donor element of point P' is ΔABC. Similarly, for all the other center points of artificial boundary triangles, their initial donor elements are obtained easily. This is one of the advantages of the overset-grid method presented in this Note.

When the rotational subzone rotates clockwise for a certain angle (for example, 150°, as shown in Fig. 2b), $\Delta A'B'C'$ moves to a new location, and we can update its new donor element by using the

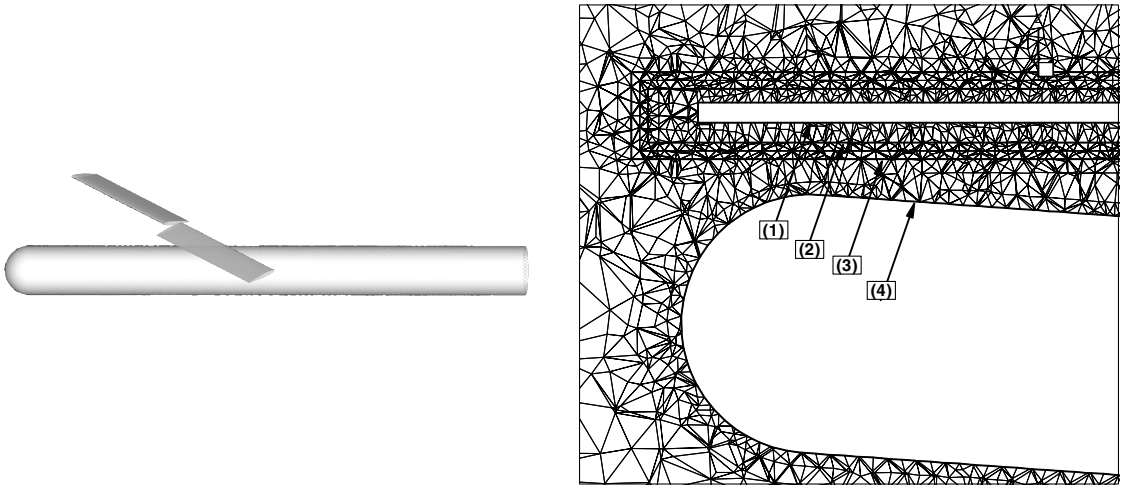

a) Overall view **b) Magnification view (slice mesh of y=0 plane)**

Fig. 1 Computational overset grids for the rotor–airframe configuration.

method of neighbor-to-neighbor algorithm [13] efficiently. So the method of searching for donor elements present above can easily get the initial donor elements and quickly update the new donor elements during the unsteady oversetting process, increasing the efficient of the overset-grid method.

C. Flow-Variable Coupling

Central to an overset scheme is the information coupling between the rotational grid and the stationary grid. The flow variables on the artificial boundary points are obtained by interpolating from the other grid overlapping with the current grid. The method of interpolation here used is based on the tetrahedron volume proportion. Suppose that the point P is an artificial boundary point whose flow variables need to be interpolated, and the tetrahedron $ABCD$ is its donor element in its overlapped grid. Then the formula of interpolating can be written as follows:

$$W_P = \alpha W_A + \beta W_B + \gamma W_C + (1 - \alpha - \beta - \gamma) W_D \tag{1}$$

where

$$\alpha = V_{BCDP}/V_{ABCD}, \qquad \beta = V_{ADCP}/V_{ABCD}$$
$$\gamma = V_{ABDP}/V_{ABCD} \tag{2}$$

D. Numerical Method

The unsteady Euler equations are discretized by a center finite volume method on the inertial coordinate system using second-order spatial accuracy. The dual-time-stepping method is adopted to advance the time-accuracy solution. Initially, a steady-state solution is obtained for a fixed rotor position based on local time stepping. Then the time-accuracy calculation is performed using the converged steady-state solution as the initial condition. At the far-field boundary, the inflow and outflow specified in the present study are based on the characteristics of the flow. On the solid surface of the rotor blades and the airframe, the flow tangency condition was applied. The density and the pressure on the solid surface were obtained by extrapolating from the interior solution.

III. Results and Discussions

The validation of the present method is made for simulating the configuration tested at Georgia Institute of Technology [14,15]. This configuration consists of a two-bladed rotor and a generic cylindrical airframe. The blades have an NACA0015 airfoil section and a rectangular planform shape with an aspect ratio of 5.3. Among the various measurement cases reported from the experiment, the one with a blade tip Mach number of 0.29 and an advancing ratio of 0.1 was chosen for validation. The blade collective pitching angle is set to 10 deg, and the rotor shaft has a forward tilt of 6 deg.

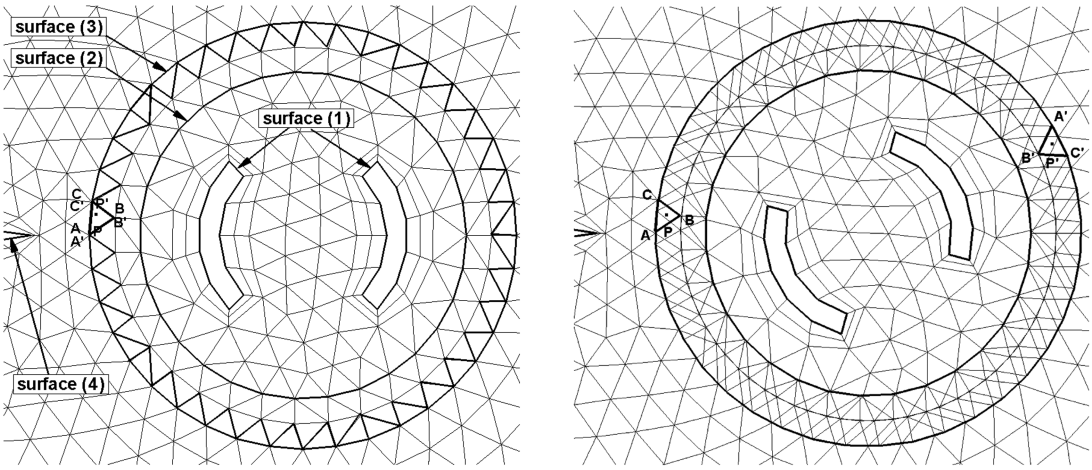

a) Initial location **b) Location after rotating for 150° clockwise**

Fig. 2 Example of 2-D coarse overset grids.

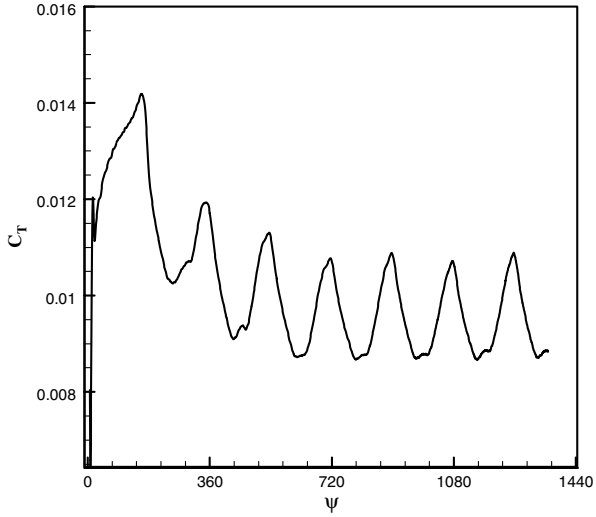

Fig. 3 Convergence of thrust coefficient.

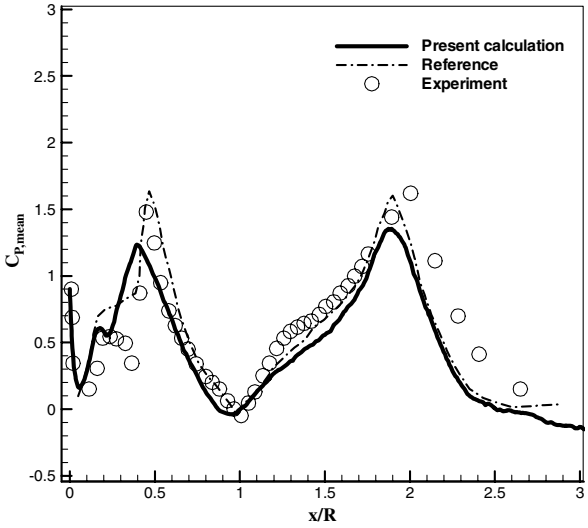

Fig. 4 Time-averaged pressure distribution along the crown line on the airframe.

During the calculating, one revolution is divided into 180 time steps, and the flow converges after two revolutions, shown in Fig. 3. The resultant thrust coefficient is 0.0095, which is a little larger than the measured 0.0091. Figure 4 shows the comparison among the computed and measured mean surface pressure distribution along the crown line on the airframe. The mean pressure distribution is obtained by averaging the instantaneous pressure over a complete cycle of revolution of the rotor. Two distinct peaks from tip-vortex impingement are observed, and it is shown that the present calculation results have lower peak values than those of the computing results from [12].

Figure 5 shows the distributions of the time-averaged streamwise and downward velocity components at 15% chord length above the airframe. The present calculation result is compared with the experimental data and the computing result from [12], and good agreements are obtained among them for both velocity components. The two peaks and steep velocity gradient from the passage of the tip vortex at the front and rear parts of the airframe are well predicted.

The time-averaged downwash distributions along the radial direction at four azimuthal positions of the rotor are presented in Fig. 6. It shows that the predicted results compare well with the experimental data and simulating results from [12] at all azimuth angles. The upwash at the front leading edge of the rotor disk is also well predicted.

The variation of the unsteady outflow velocity observed at a fixed point located at 67% span and 67.5° azimuth angle is compared with the experiment and calculating results from [12] in Fig. 7. The measurement is made at 15% chord length below the rotor disk plane. The figure shows that the overall variation of the velocity and the sharp spikes from the blade passage are generally in good agreement with the experiment. However, the magnitudes of the spikes of present results are a little lower than those of experiment, and the phases of the spikes are a little off from those of the experiment. Compared with the reference results, the present has a closer value to the experiment for the magnitudes of the spikes, and the two numerical results have almost the same spike phase.

In Fig. 8, the instantaneous pressure distributions along the crown line of the airframe are presented for two typical blade azimuth angles. It shows that the predicted overall pressure variations in time and in space compare well with the experiment and numerical results of [12] for both azimuth angles. The effect of the blade passage is well predicted, as shown with a high pressure rise at the nose region of the airframe at zero blade azimuth angle. However, the local pressure spike associated with the tip-vortex impingement observed

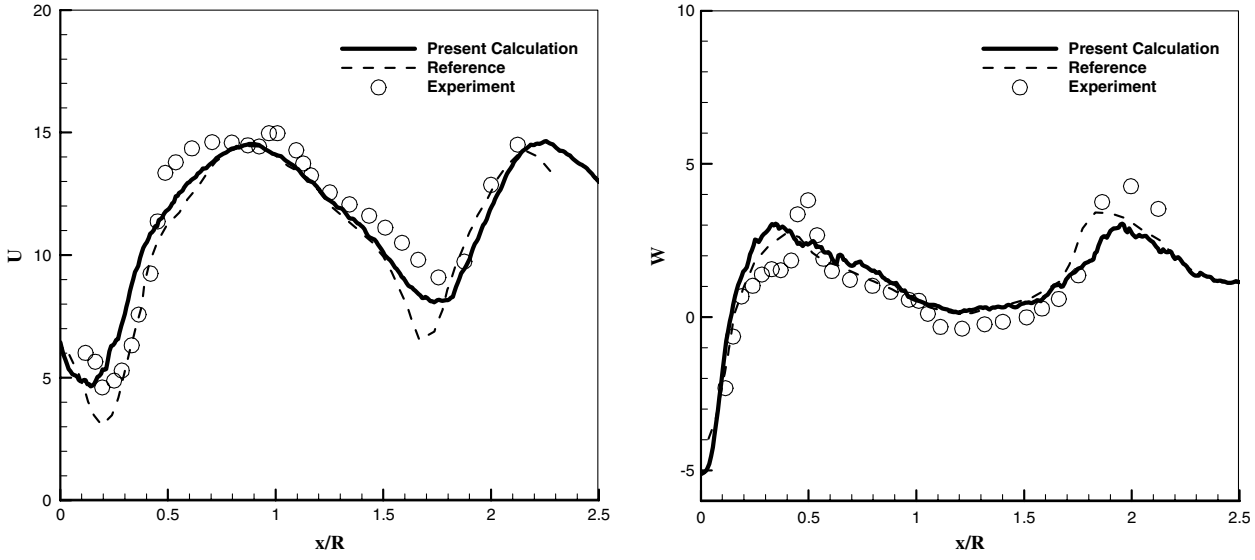

a) Streamwise velocity component **b) Downward velocity component**

Fig. 5 Time-averaged velocity distributions at 15% chord length above the airframe.

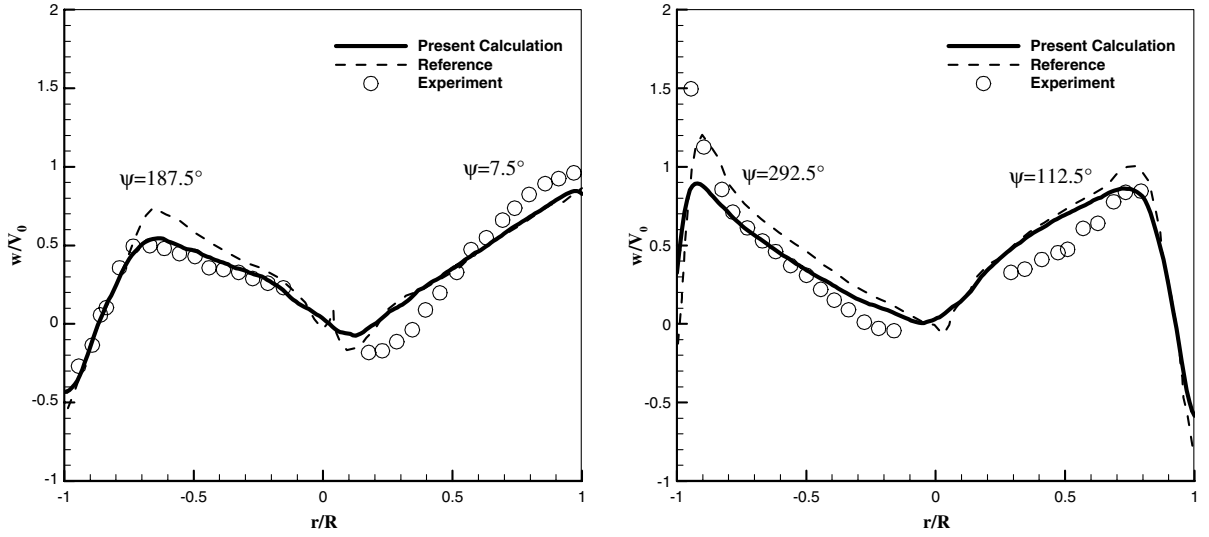

a) Along ψ=7.5° and ψ=187.5° b) Along ψ=112.5° and ψ=292.5°

Fig. 6 Time-averaged downwash distributions at 15% chord length below the rotor disk (positive downward).

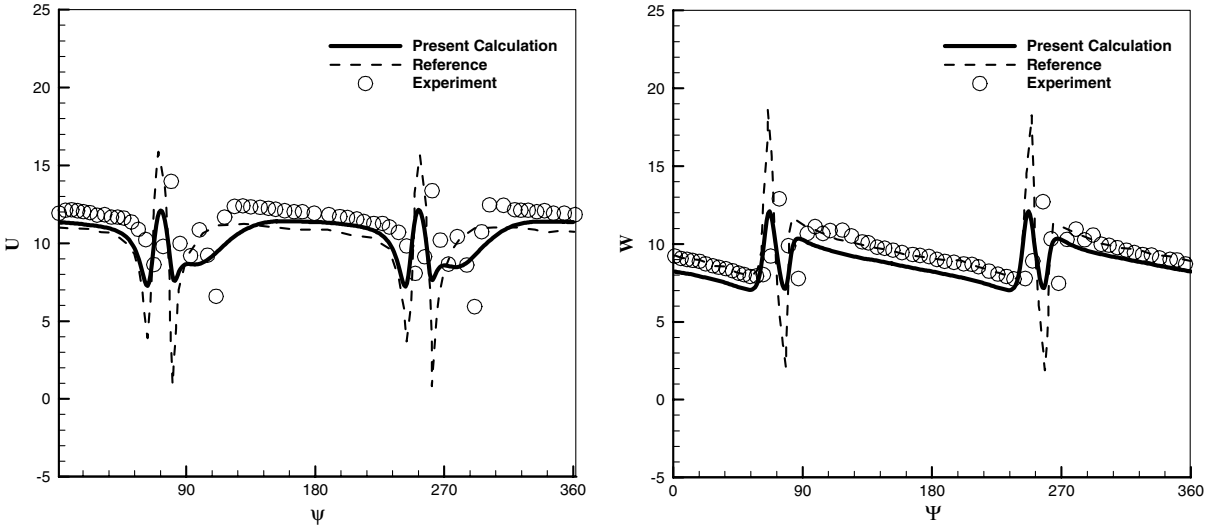

a) Streamwise velocity component b) Downward velocity component

Fig. 7 Unsteady outflow variations observed at $r/R = 0.667$, $\Psi = 67.5°$, and 15% chord length below the rotor disk plane.

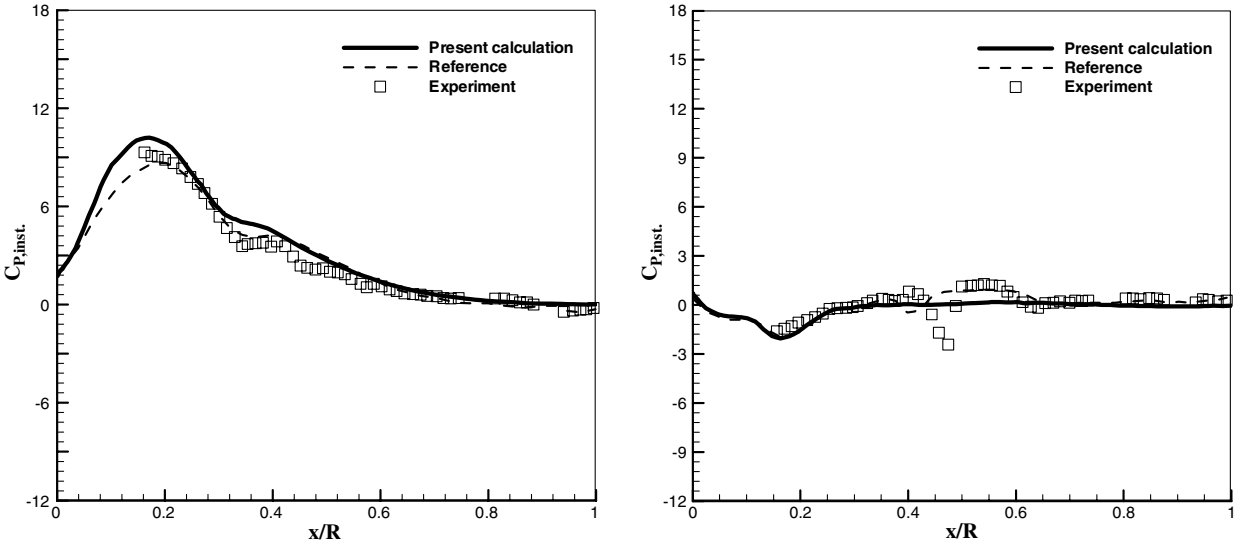

a) ψ=0° b) ψ=90°

Fig. 8 Instantaneous surface pressure distributions along the crown line of the airframe.

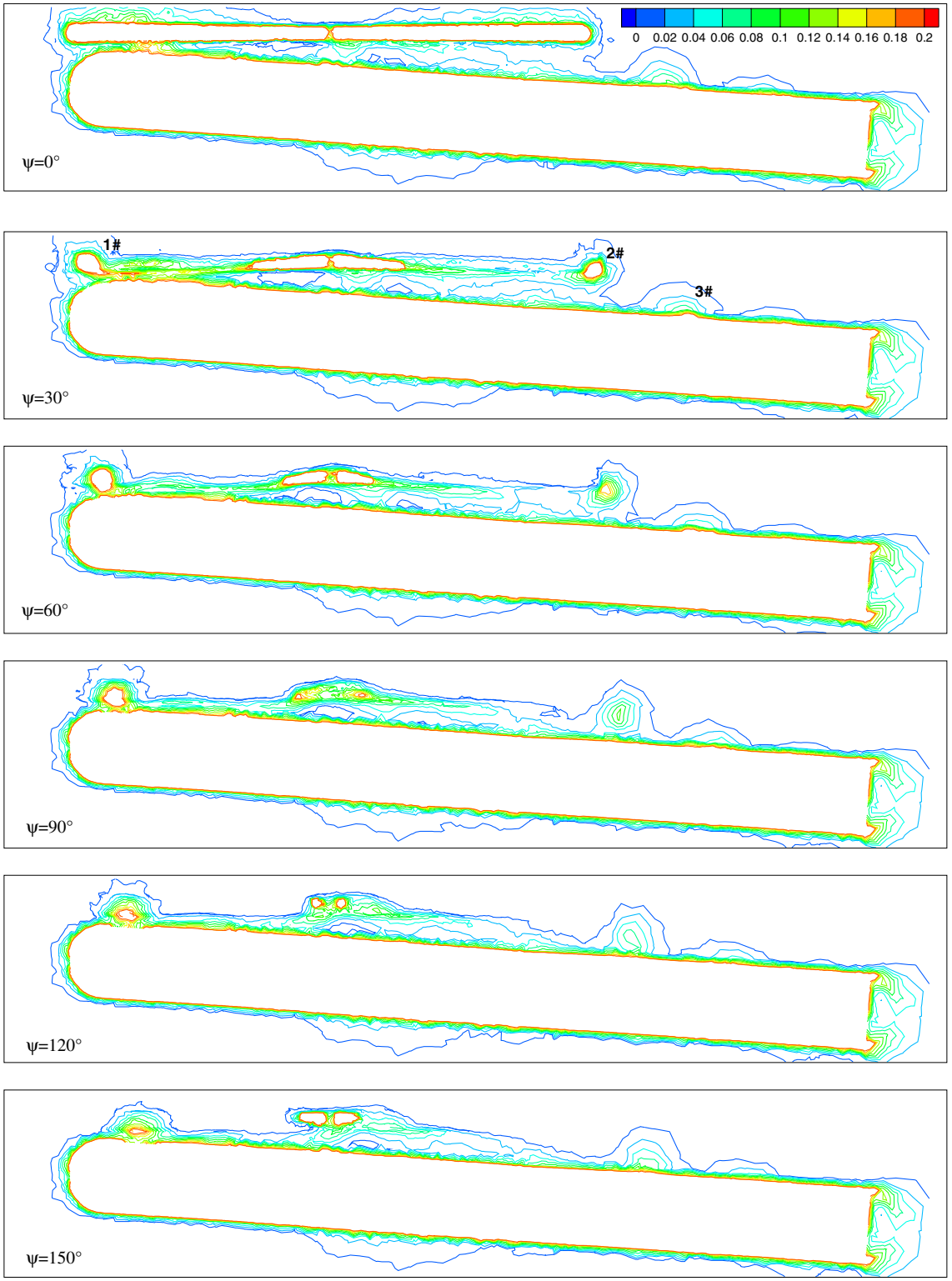

Fig. 9 Instantaneous vorticity contours at the airframe symmetric plane.

by the experiment at the downstream is not properly resolved from the present calculation and the reference computing.

In Fig. 9, the instantaneous vorticity contours at the airframe symmetric plane are presented for six blade azimuth angles. It shows that the overall mechanism of the generation of the tip vortex, its subsequent migration, and the impingement on the airframe is well demonstrated using the present unstructured overset grids. The inboard vortex sheets emanating from the blade trailing edge are also well captured. The convection of the highly vertical flow across the overlapping area is also well confirmed in the figure.

In Fig. 10, the perspective view of the instantaneous isovorticity surface is presented. The formation of the trailing tip vortex, its migration to the downstream of the rotor, and the impingement of the tip vortex on the fuselage can be observed in the figure. The formation of a rotor disk vortex that is similar to the tip vortex of fixed wings is also clearly demonstrated.

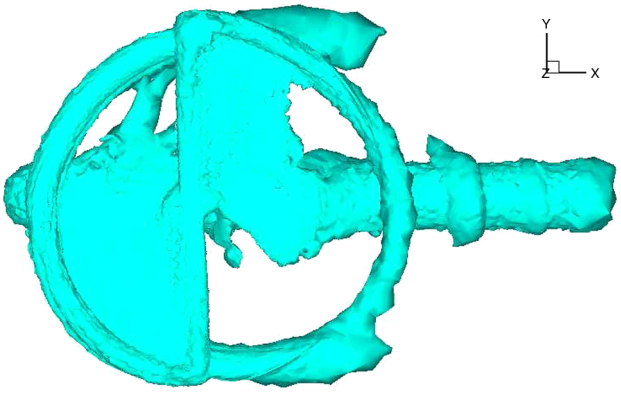

Fig. 10 Instantaneous isovorticity surface for the Georgia Tech configuration.

IV. Conclusions

The rotor–airframe unsteady interaction aerodynamic is simulated by solving the three-dimensional unsteady Euler equations based on the unstructured overset grids. The method of unstructured mesh can easily handle the complex geometries, and the overset grids can treat the relative motion of helicopter rotor–airframe interaction effectively by dividing the flowfield into two overset subzones. Validation is made by simulating the Georgia Tech rotor–airframe interaction configuration and comparing the predicted results with those of the experimental data. The predicted time-averaged and time-accurate inflow and airframe surface pressure distribution compare well with experimental data and calculating results of other researchers. It is demonstrated that the presented unstructured overset grids are effective and robust for simulating unsteady rotor–airframe aerodynamic interaction. The application of the present method to more complicated configurations, such as coaxial rotor helicopter, helicopter with tail rotor, aircraft with two propellers, and so on, will be investigated in the future work.

Acknowledgments

This work was supported by Chinese Postdoctoral Science Foundation and National Key Laboratory of Science and Technology Foundation of China (9140C42010210ZS51).

References

[1] Berry, J. D., "Prediction of Time-Dependent Fuselage Pressure in the Wake of a Helicopter Rotor," *Proceedings of the Eighth European Rotorcraft Forum*, Paris, Aug.–Sept. 1992.

[2] Lorber, P. F., and Egolf, T. A., "An Unsteady Helicopter Rotor-Fuselage Aerodynamic Interaction Analysis," *Journal of the American Helicopter Society*, Vol. 35, No. 3, 1990, pp. 32–42. doi:10.4050/JAHS.35.32

[3] Whitfield, D. L., and Jameson, A., "Euler Equation Simulation of Propeller-Wing Interaction in Transonic Flow," *Journal of Aircraft*, Vol. 21, No. 11, 1984, pp. 835–839. doi:10.2514/3.45052

[4] Zori, L. A. J., and Rajagopalan, R. G., "Navier–Stokes Calculations of Rotor–airframe Interaction in Forward Flight," *Journal of the American Helicopter Society*, Vol. 40, No. 2, 1995, pp. 57–67. doi:10.4050/JAHS.40.57

[5] Chaffin, M. S., and Berry, J. D., "Helicopter Fuselage Aerodynamics Under a Rotor by Navier–Stokes Simulation," *Journal of the American Helicopter Society*, Vol. 42, No. 3, 1997, pp. 235–243. doi:10.4050/JAHS.42.235

[6] Pandya, M. J., Bhat, M., and Parikh, P., "Application of Unstructured Grid Methodology to Rotorcraft Flows," *Technical Specialists' Meeting for Rotorcraft Acoustics and Aerodynamics*, AHS International, Alexandria, VA, Oct. 1997.

[7] Lee, J.-K., and Kwon, O. J., "Prediction Aerodynamic Rotor-Fuselage Interactions by Using Unstructured Meshes," *Transactions of the Japan Society for Aeronautical and Space Sciences*, Vol. 44, No. 146, 2002, pp. 208–216. doi:10.2322/tjsass.44.208

[8] Boyd, D. D., Jr., Barnwell, R. W., and Gorton, S. A., "A Computational Model for Rotor-Fuselage Interactional Aerodynamics," 38th AIAA Aerospace Sciences Meeting and Exhibit, AIAA Paper 2000-0256, Reno, NV, Jan. 2000.

[9] Tadghighi, H., "Simulation of Rotor-Body Interactional Aerodynamics: An Unsteady Rotor Source Distributed Disk Model," *57th Annual Forum Proceedings*, AHS International, Alexandria, VA, May 2001.

[10] Hariharan, N., and Sankar, L. N., "Unsteady Overset Simulation of Rotor–Airframe Interaction," *Journal of Aircraft*, Vol. 40, No. 4, 2003, pp. 662–674. doi:10.2514/2.3170

[11] Kang, H. J., and Kwon, O. J., "Unstructured Mesh Navier–Stokes Calculations of the Flowfield of a Helicopter Rotor in Hover," *Journal of the American Helicopter Society*, Vol. 47, No. 2, 2002, pp. 90–99. doi:10.4050/JAHS.47.90

[12] Nam, H. J., Park, Y. M., and Kwon, O. J., "Simulation of Unsteady Rotor-Fuselage Aerodynamic Interaction Using Unstructured Adaptive Meshes," *Journal of the American Helicopter Society*, Vol. 51, No. 2, 2006, pp. 141–149. doi:10.4050/JAHS.51.141

[13] Loehner, R., "Robust Vectorized Search Algorithms for Interpolation on Unstructured Grids," *Journal of Computational Physics*, Vol. 118, No. 2, 1995, pp. 380–387. doi:10.1006/jcph.1995.1107

[14] Liou, S. G., Komerath, N. M., and McMahon, H. M., "Velocity Measurements of Airframe Effects on a Rotor in Low-Speed Forward Flight," *Journal of Aircraft*, Vol. 26, No. 4, 1989, pp. 340–348. doi:10.2514/3.45766

[15] Brand, A. G., McMahon, H. M., and Liou, S. G., "Surface Pressure Measurements on a Body Subject to Vortex Wake Interaction," *AIAA Journal*, Vol. 27, No. 5, 1989, pp. 569–574. doi:10.2514/3.10147